UCRL-101871
PREPRINT

PROPAGATION OF FLUID-DRIVEN FRACTURES IN JOINTED ROCK. PART 2: PHYSICAL TESTS ON BLOCKS WITH INTERFACE OR LENS

S. C. Blair
R. K. Thorpe
F. E. Heuze

This paper was submitted for publication in the
International Journal of Rock Mechanics and Mining Science

September, 1989

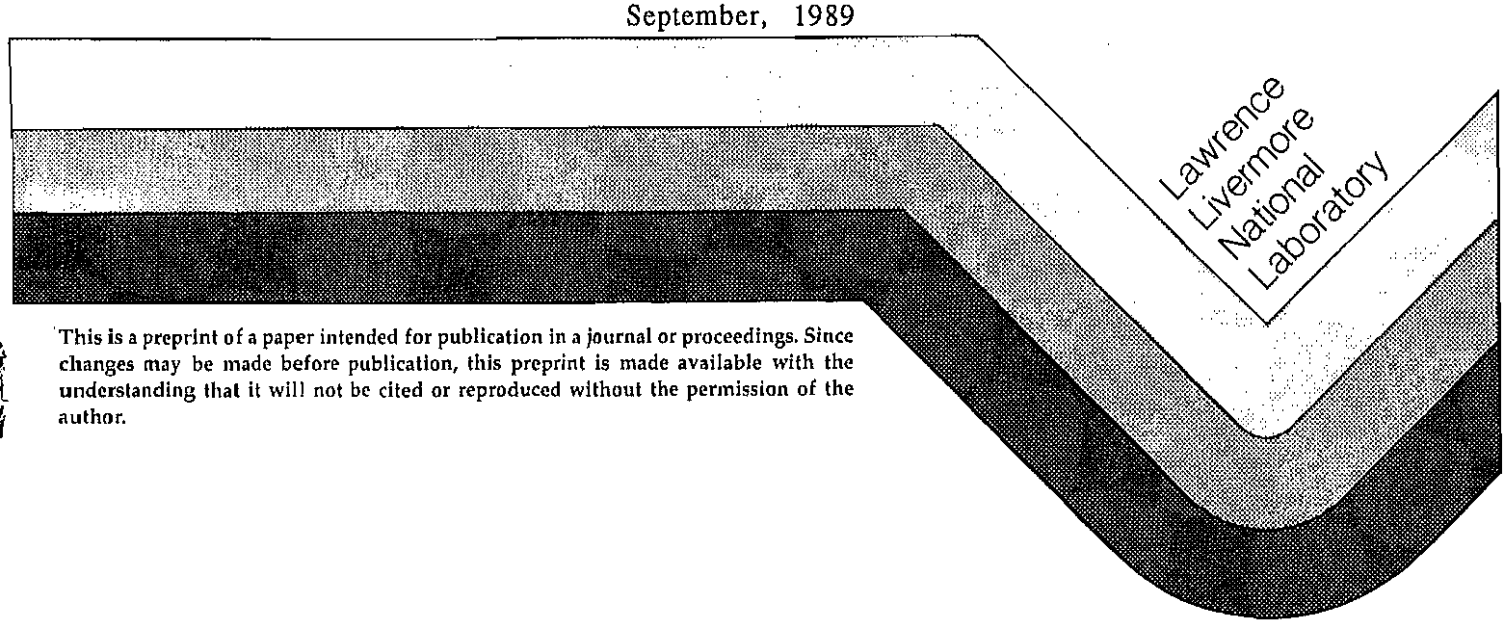

INDEX

ABSTRACT

As introduced in Part 1 of this paper, we have pursued a dual - numerical and experimental - modeling program to gain insight in the interaction of induced, fluid-driven fractures with natural discontinuities in rock masses. This is a topic of interest in the stimulation of oil and gas reservoirs, as well as geothermal fields. It is also relevant to the disposal of liquid wastes underground and the estimation of in-situ stresses, both by hydrofracturing.

The experimental program was composed of two series of tests on blocks of rock simulants loaded biaxially. The first one is denoted "interface tests". It was performed at the time of the development of the steady-state, coupled fracture and flow numerical model, for the purpose of validation. The blocks were hydrofractured while loaded biaxially. These tests provided information only as to whether cracks had crossed the interface between the two parts of the blocks, or not. No time-dependent data or fracture path data were obtained during the tests. The fracture trajectories were determined from post-test dissections of the blocks.

The second, more sophisticated, test series will be denoted "lens tests". Sandstone lenses were embedded in hydrostone blocks which were fractured with single-wing fluid-driven cracks, while under a triaxial external loading. Fluid pressure and crack front were tracked as a function of time. This series had a two-fold purpose: to provide a validation basis for the new, time-dependent, numerical developments, and to provide forward diagnostics, on the pressure-time records, of the interaction of hydrofractures with embedded lenses. The physical testing was successful on both counts. In particular, the pressure-time records showed clear pressure discontinuities associated with the passage of the hydrofracture into the lens.

1. INTRODUCTION

In Part 1 of this paper, we have provided the background and the rationale for our joint numerical and experimental program aimed at gaining insights in the interaction of induced fluid-driven fractures and natural discontinuities in rock masses. In this Part 2 we will describe in detail two series of physical tests on blocks of rock simulants. Physical modeling is a proven way to provide a measure of validation of mathematical modeling; moreover, it can provide its own diagnostics which can be directly relevant to the behavior of a prototype. There is a modest data base of scaled physical experiments on rocks or rock simulants, concerning hydrofracturing in jointed media [1-7], or gas-driven borehole fracturing [8-10]. However, none of them provided time-dependent records of fracture-front position versus borehole pressure. Our second group of block experiments [11] represented a much more sophisticated attempt to obtain such information, and it was successful in that regard.

The first test series will be denoted "interface tests". It was performed at the time of the development of the steady-state, coupled fracture and flow numerical model, for the purpose of validation. The blocks were hydrofractured while loaded biaxially. These tests provided information only as to whether cracks had crossed the interface between the two parts of the blocks, or not. No time-dependent data or fracture-path data were obtained during the tests. The fracture trajectories were determined from post-test block dissections.

The second, more sophisticated, test series will be denoted "lens tests". Sandstone lenses were embedded in hydrostone blocks which were fractured with single-wing fluid-driven cracks, while under a triaxial external loading. Fluid pressure and crack front were tracked as a function of time. This series had a two-fold purpose: to provide a validation basis for the new, time-dependent, numerical developments, and to provide forward diagnostics, on the pressure-time records, of the interaction of hydrofractures with embedded lenses.

The following two chapters provide the details of the tests performed and their results. The "lens tests" will be emphasized.

2. THE "INTERFACE" TESTS SERIES

2.1 Overview

The basic test layout and the test setup are shown in Figures 1 and 2. For reasons of time and budget, this series of experiments was kept simple in the sense that we seeked only to determine whether or not, under certain conditions of material properties, interface properties, and external stresses, the hydrofrac would cross the interface.

Hydraulic fractures were initiated by means of an oil injection tube embedded fairly close to the interface. Cracks generally propagated in the direction of the maximum applied load, intersecting the interface at either 30 or 60 degrees. A total of 16 tests were completed with normal stresses on the interfaces ranging from 3.8 to 10.6 MPa. A crack typically crossed an interface when the normal stress exceeded 8.7 MPa, regardless of which material it originated in. Two- and three-dimensional finite element models of the blocks indicated that a condition of plane stress prevailed at the outset of testing. They also showed that, for a given total boundary load, stresses on the interface were generally insensitive to the details of load distribution. However, concentrated stresses at the injection point proved to be substantially different from what would be calculated by assuming a uniform internal stress field in the block [12].

2.2 Material Characterization

2.2.1 Solid materials

After a review of modeling material literature and a few trials, we selected two model materials

A: 100% gypsum cement with a 33% water/cement weight ratio

B: 70% gypsum cement + 30% Monterey sand No. 00, with the same water/cement ratio.

A series of tests was performed for mechanical characterization, including the determination of fracture toughness with the short-rod system [13,14]. The results are summarized in Table 1.

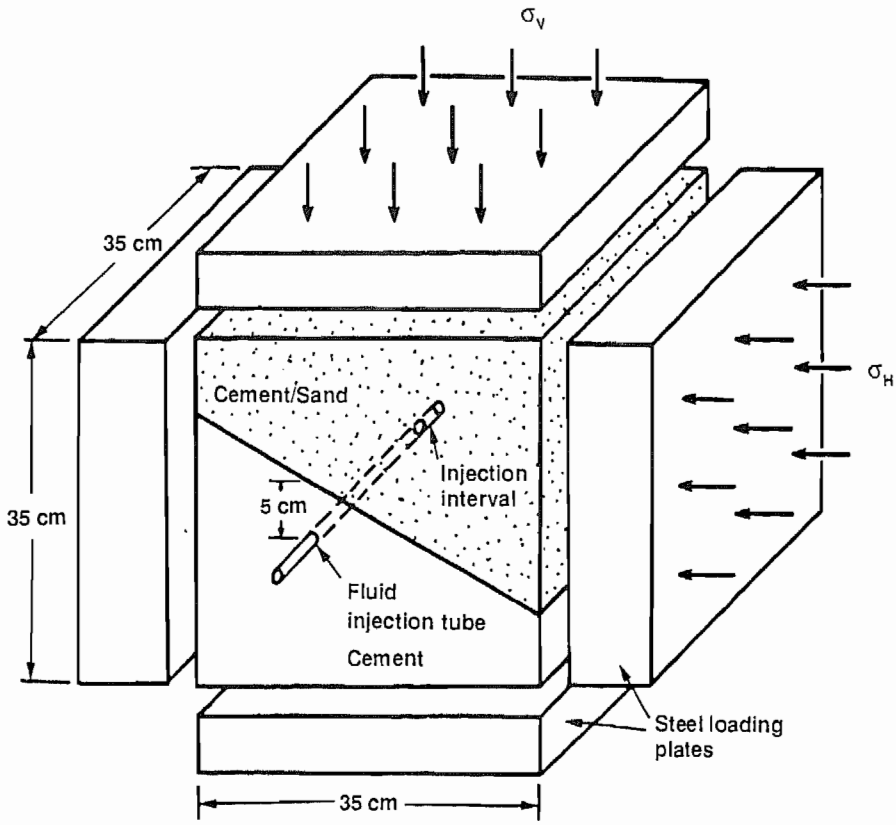

Figure 1. Schematic Diagram of Experiments.

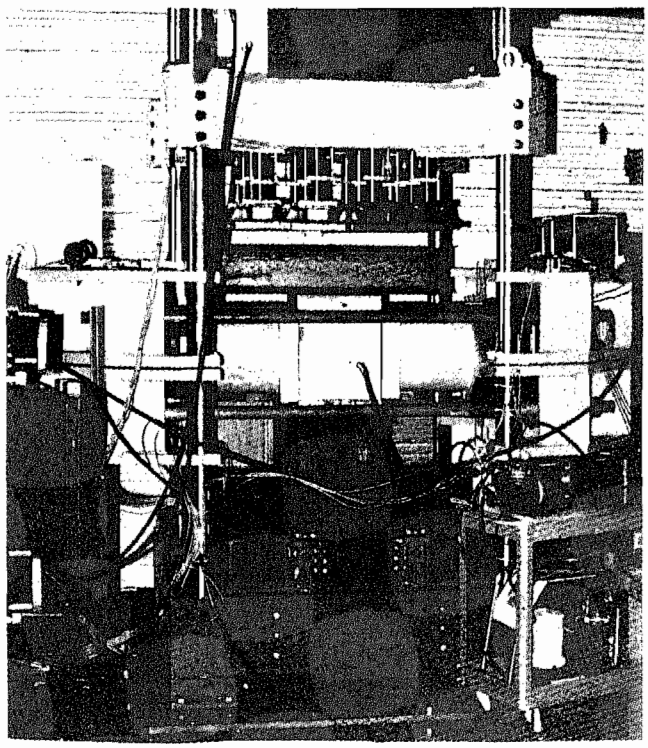

Figure 2. Experimental Equipment and Setup.

Table 1. Summary of Results of Materials Characterization Tests.

Material	Density (g/cm^3)	Modulus of Elasticity (GPa)	Poisson's Ratio	Tensile Strength (MPa)	Uncon. Comp. Strength (MPa)	Fracture tough. ($MPa\cdot\sqrt{m}$)
A	1.54	14.3	0.23	3.10	36.9	0.502
B	1.83	17.9	0.19	1.52	33.6	0.469

2.2.2 Interfaces

Frictional properties of the interfaces between materials A and B were determined with the direct shear system, shown in Figure 3. Samples for these tests were cast in 25.4 x 40.6 cm wooden molds with the interfaces located at midsection and parallel to the bottom of the mold. Each interface possessed some small but undetermined degree of cohesion; therefore, the two halves of each specimen were separated prior to testing to yield unbonded interfaces. The area of each interface was 1030 cm^2, which is comparable to that of the hydrofracturing blocks. The machine was equipped with transducers to record shear and normal displacements; the shear and normal forces were monitored by strain gage load cells. The peak and residual shear strength envelopes from 5 shear tests are shown in Figure 4. The shear stiffness was obtained from the shear tests; it varied with the applied constant normal stress as:

Table 2. Shear Stiffness of Interface.

Test	1	2	3	4	5
σ const (MPa)	0.83	0.64	0.44	0.20	0.11
K_s (GPa/m)	8.1	8.1	7.8	4.6	4.3

For normal stiffness estimates, the shear system normal deformation measurements were judged too imprecise. Instead, an interface was created by casting the A and B materials in a cylinder 7.1 cm in diameter and 16.3 cm tall, so that the interface was normal to the axis and midway through the sample. An axial compression test was performed, and the sample deformed linearly from 3.45 MPa to the maximum applied normal stress of 6.9 MPa. The joint deformation was obtained from the linear part of the record, after subtracting the deformation of the solid materials estimated from

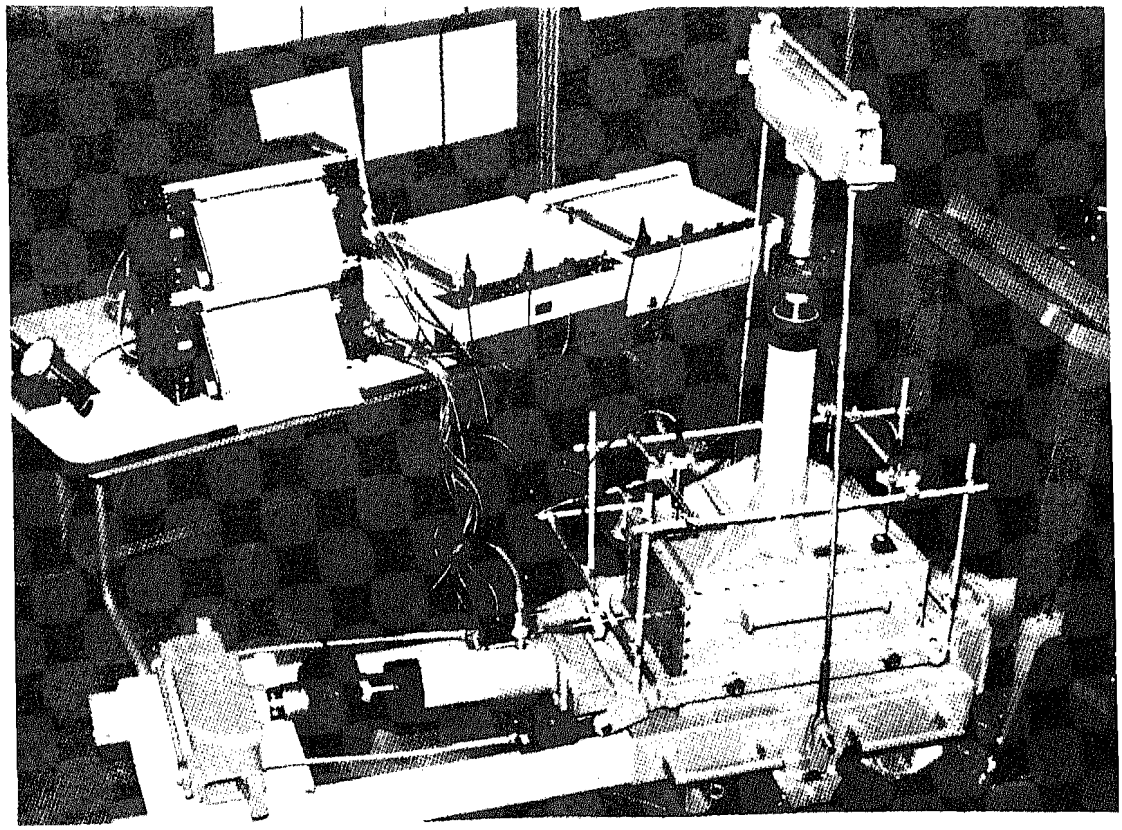

Figure 3. Direct Shear Testing Apparatus

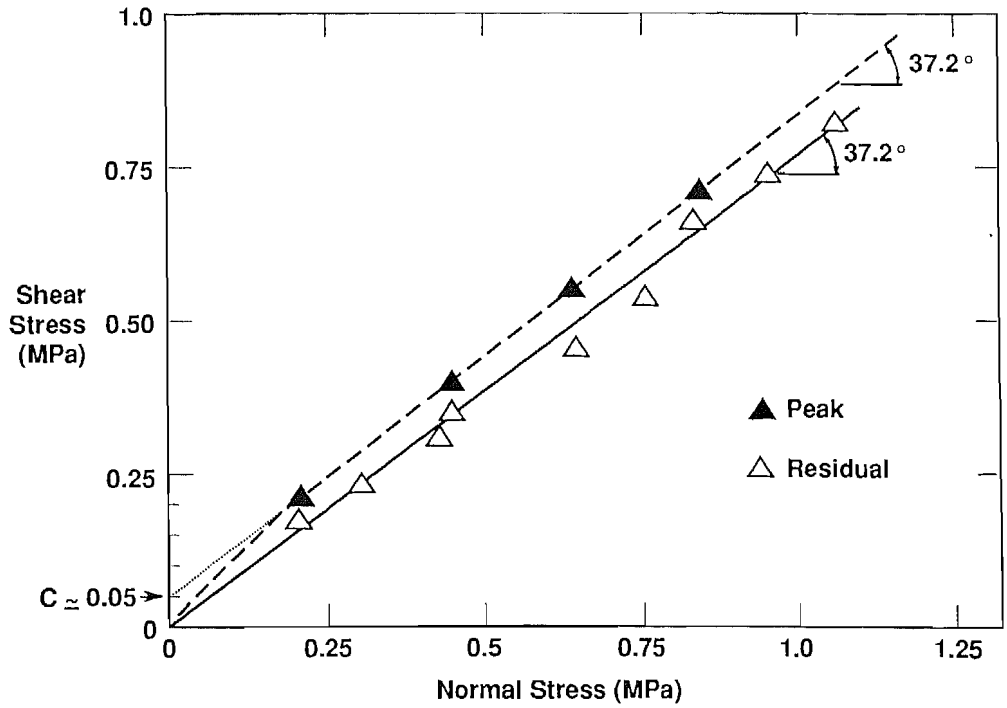

Figure 4. Peak and Residual Shear Strength Envelopes.

the known moduli. The resulting normal stiffness for the A/B interface was K_n = 71.6 GPa/m.

2.3 Hydrofracturing Test Procedure

The 35 cm two-material cubes were loaded biaxially in a hydraulic press under a horizontal stress, σ_h, and a vertical stress, σ_v. The third pair of faces, one of which contained the fluid injection tube, was not loaded. The normal to the interface separating the two materials was inclined so that it formed an angle of either 30° or 60° to the major principal stress axis.

The blocks were cast in molds made of aluminum plates held together by threaded screws. The mold was tilted at 30° while one half of a block was poured with the first material, usually the 70/30 cement/sand mixture. When this had set for three to four hours, the molds were placed upright and the remaining half of the block was cast with pure cement (100/0). After 24 hours, the molds were removed. The top surface of the second casting was machined flat. All blocks cured in air at least ten days before being used in a test. A fluid injection point was provided by drilling a 0.711-cm diameter hole to a depth of about 16.5 cm, into the block. The perpendicular distance from this hole to the interface was about 3.8 cm. A smaller diameter hole (.64 cm) and 1.27 cm long was drilled at the bottom of the first hole. A steel high-pressure injection tube then was bonded with epoxy within the injection hole. A small o-ring was glued on the end of the injection tube and rested on the shoulder near the bottom of the borehole where the diameter decreased. After the epoxy was applied to the tube and the tube inserted into the borehole, a lead weight was applied to the top of the tube so that the o-ring was compressed during curing of the epoxy.

Pressurization of the injection interval was done by means of a two-stage nitrogen-to-oil intensifier. Medium-heavy oil (viscosity about 300 cp) was used as the fracturing fluid; however, some air inevitably was trapped within the borehole at the start of a test. Oil pressure was monitored at the intensifier, rather than at the borehole, and recorded as a function of time. Because the pressure intensifier was activated by nitrogen, injection rates could not be controlled. The resulting pressurization rates varied from about 0.7 to 1.7 MPa/sec.

2.3 An Analysis of Internal Block Stresses

The loading in the large biaxial frame of Figure 2 was not expected to be identical to a perfect stress loading on the block faces, because of the rigidity of the loading platens, and because the discrete interfaces between the platens and the blocks somewhat restrained block movement. Also, the blocks were truly three-dimensional, so that a 2-D approximation of plane stress or plane strain could be incorrect. Then, how did the actual stress distribution inside the blocks compare to the ideal distribution expected under perfect stress loading of their faces? To gain insight into this matter, one of the load cases (11.0 MPa vertical, 5.2 MPa horizontal) was examined by both 2- and 3-dimensional finite element analyses. In both the 2-D and 3-D models the interface within the block and the four external (block/steel) interfaces were represented by discrete joint elements.

The 2-D mesh for the plane stress FEFFLAP [15,16] analysis had 416 nodes and 141 elements. The structure is shown on Figure 5, with magnified deformations. This reveals the tendency for slippage of the upper half-block. The 3-D analysis of the jointed block was performed with a 3-D jointed finite element code which was developed by C. St. John at Imperial College, London [17]. It was modified by F. Heuze to include non-linear joint behavior, and to operate in large core memory on the CDC 7600 computers at LLNL. The basic-3-D model is shown in Figure 6; it had 440 nodes and 288 elements. The model was run with 2 materials, and the loads were applied with the steel platens and pistons, as in the physical tests. Figure 7 represents an x-z cross section through the middle of the block. Results specific to the 3-D analysis are: (1) the stresses near the slanted interface and the boreholes are not very sensitive to the manner in which the total load was distributed on the outside of the steel platens, and (2) the out-of-plane stress at the hydrofrac initiation location is about 0.1 MPa in compression. This is very close to plane stress, as opposed to a plane strain value of $\sigma_y = \nu(\sigma_x + \sigma_z) = 3.2$ MPa.

Under ideal biaxial loading, the normal stress on the interface is nominally 9.57 MPa, whereas the 3-D results in Figure 7 show it to be 8.69 MPa. While this difference of about 10 percent is not large, the error involved in calculating the nominal shear stress is pronounced. For the given load conditions, the 2-D and 3-D analyses gave remarkably similar shear stresses of about 0.87 MPa on the interface. The nominal shear stress, however, would be 2.54 MPa. This difference of nearly 300 percent

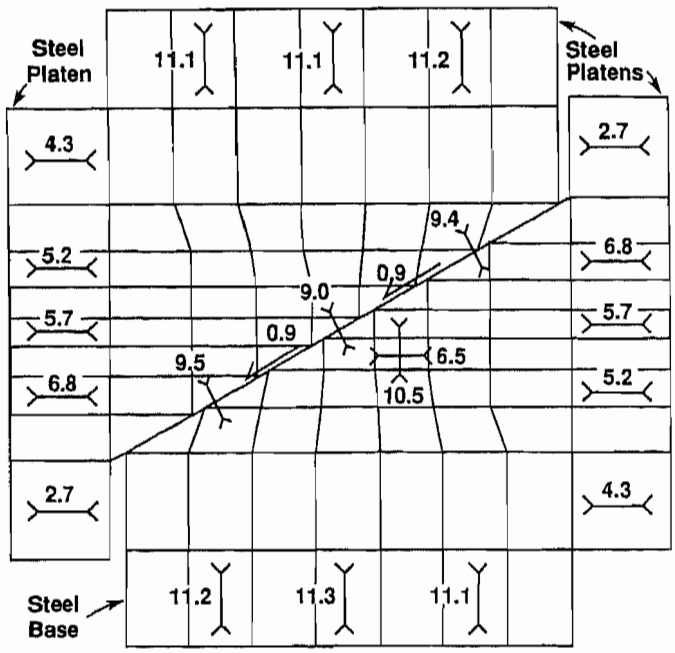

Figure 5. 2-D, Plane Stress, Model of Experimental Block.

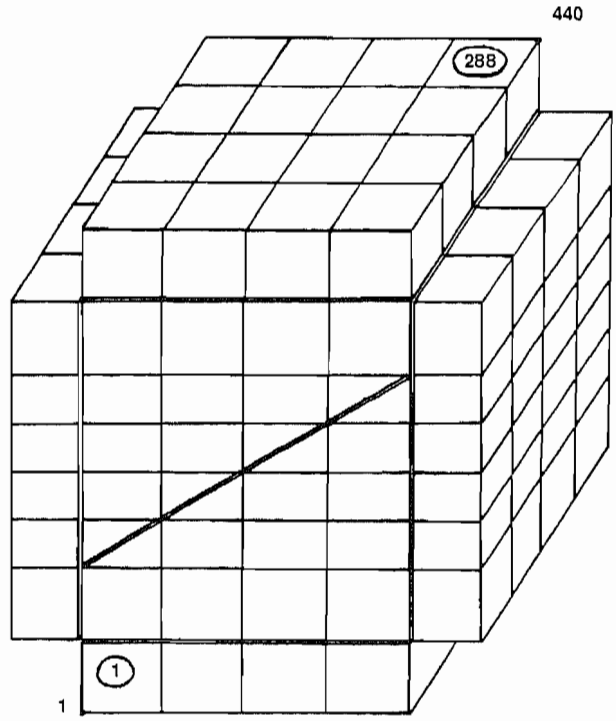

Figure 6. 3-D Finite Element Model of Experimental Block.

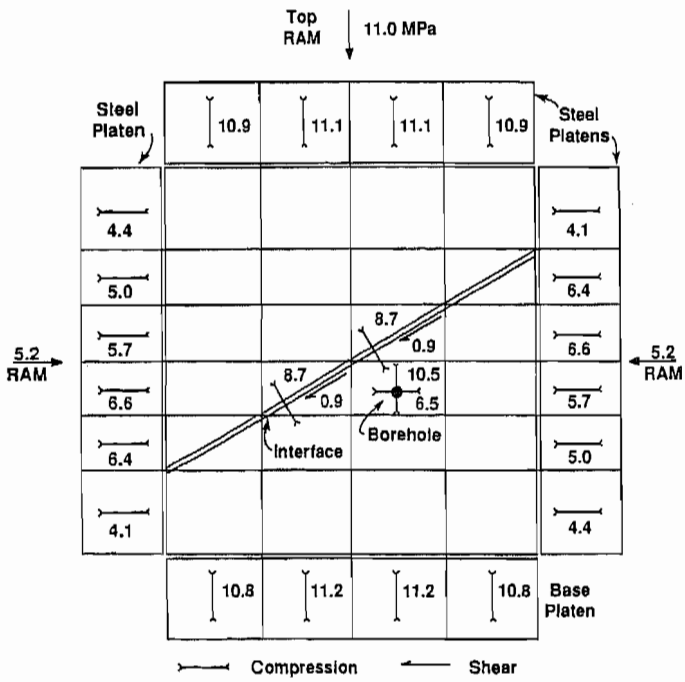

Figure 7. Cross-Section Through Middle of 3-D Model.

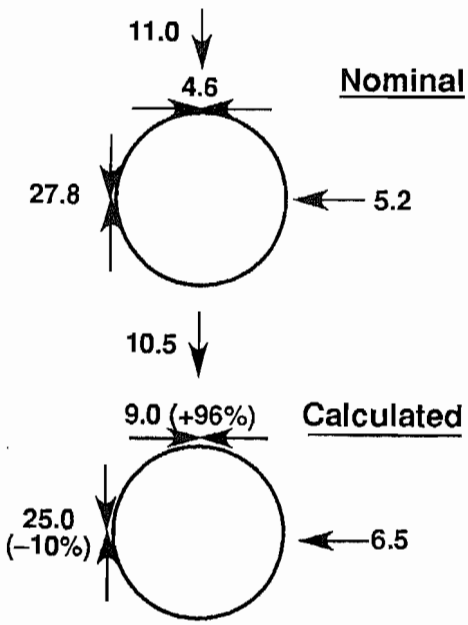

Figure 8. Nominal and Calculated Stress Conditions at Injection Point.

underscores the need for correctly accounting for the frictional behavior of the interface. Moreover, the state of stress at the borehole location is not what would be predicted from the boundary conditions of σ_x = 5.2 MPa and σ_z = 11.0 MPa. The σ_z is within 5%, but because of the bending of the vertical platens, the σ_x is 6.5 MPa vs. 5.2 nominal. When the hole concentrates stresses tangentially, the difference is amplified as shown in Figure 8. This certainly would affect the expected fracture initiation pressure.

2.5 Test Results and Discussion

The results of the 16-test series are summarized in Table 3, in chronological order. Typically we tried to perform 2 hydrofracture tests per block, so as to change the medium of initiation. For some of the tests we also changed the angle of incidence of the hydrofracture with the interface. In Table 3, α is the angle of the hydrofracture with the normal to the interface.

Throughout the test series it was intended that the hydraulic fractures would initiate and propagate in a plane parallel to the injection tube and σ_1. However, this was not the only pattern to develop. Instead, three basic types of fractures were observed and examples of each are shown in Figure 9, a photograph of Block 8 (Tests H-13 and 14). The first, labeled Type 1, generally had the desired orientation. Type 2 initiated parallel to the injection tube, but curved sharply until most of the fracture face was approximately parallel to the free, or unloaded pair of block faces. The third type initiated roughly perpendicular to the injection tube, usually at the bottom of the hole, and remained parallel to the unloaded faces over its full extent.

It is clear that the orientation of fractures was strongly influenced by the three-dimensional stress field. This makes an analysis of the interaction of a crack with an interface a difficult matter in two dimensions. However, in the immediate vicinity of the injection hole, a 2-D approach may be warranted, given that 15 of the 16 tests involved cracks that initiated parallel to the borehole (Types 1 or 2). As shown in Table 3, seven of these Type 1 or 2 cracks passed through the interface, but only at normal stresses in excess of 5.9 MPa.

Although they are discussed at some length in [8], the injection pressure-time record did not yield much insight into the behavior of the fractures. For validation of the

Table 3. Summary of Hydrofracturing Results

Expt. No.	Block No.	σ_1 (MPa)	σ_2 (MPa)	α (deg)	Nom. σ_N (MPa)	Tube Location Material	Interface Interaction[b]
H-1	1	4.8	.59	30	3.8	70/30	2-stopped
H-2	2	4.8	.69	30	3.8	100/0	1-stopped
H-3	3[a]	7.6	1.03	30	5.9	70/30	1-stopped 3-crossed
H-4	3[a]	7.6	1.03	30	5.9	100/0	1-stopped
H-5	4	11.0	5.2	30	9.6	70/30	2-crossed
H-6	4	11.0	5.2	30	9.6	100/0	3-crossed
H-7	5	11.0	5.2	30	9.6	70/30	2-did not reach 3-crossed
H-8	5	11.0	5.2	30	9.6	100/0	2-did not reach 3-crossed
H-9	6	12.4	5.2	30	10.6	70/30	2-crossed
H-10	6	12.4	5.2	30	10.6	100/0	1-crossed 3-crossed
H-11	7[a]	12.4	5.2	30	10.6	100/0	2-crossed
H-12	7[a]	12.4	5.2	30	10.6	70/30	2-crossed
H-13	8[a]	12.4	.07	30	9.3	70/30	2-crossed 3-crossed
H-14	8[a]	12.4	.07	30	9.3	100/0	1-crossed
H-15	9[a]	15.2	.07	60	3.8	70/30	1-did not reach 3-crossed
H-16	9[a]	15.2	.07	60	3.8	100/0	1-stopped

[a]Interface was intact prior to and during tests

[b]See text for description of fracture types.

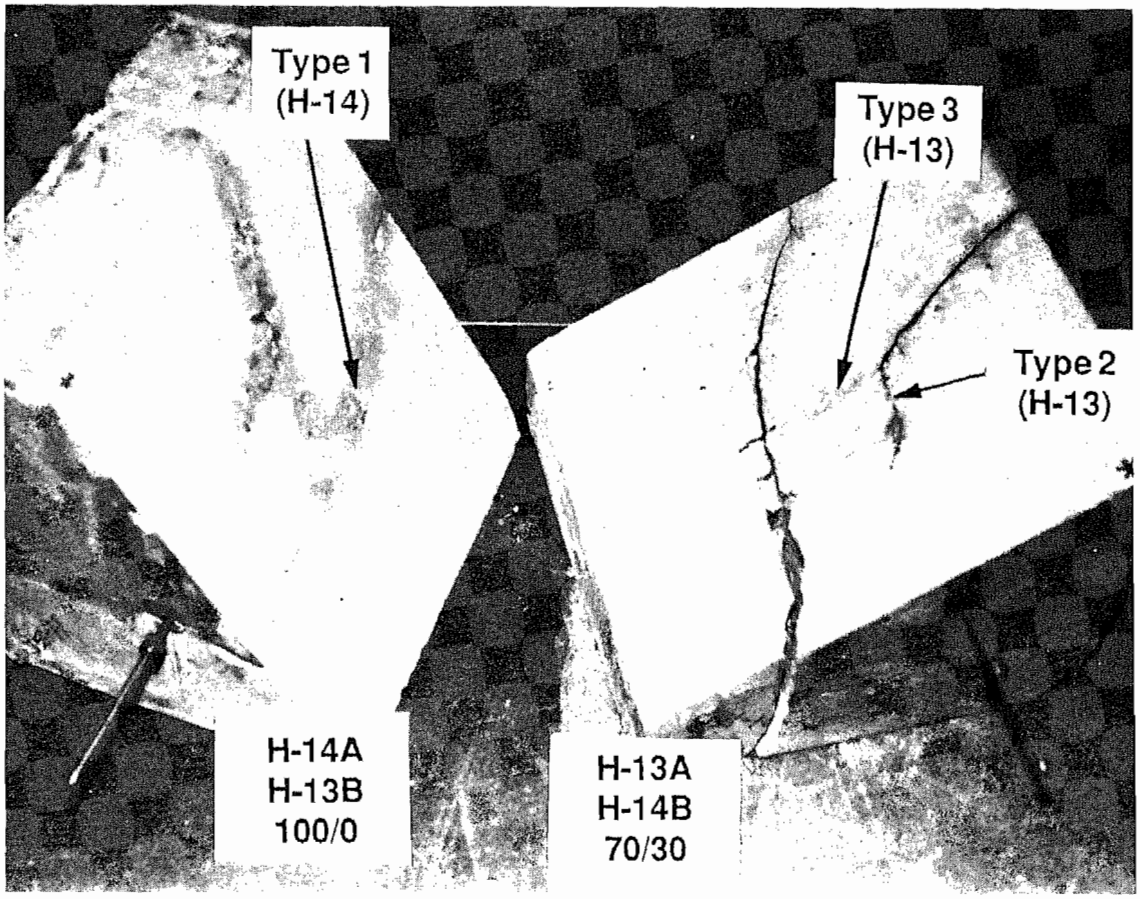

Figure 9. Post-Test Photograph of Block 8, Tests H-13 and H-14.

numerical models, we decided to select two tests, H-2 and H-10 in which type 1 fractures had either stopped at or crossed the interface. As discussed in the companion paper, the FEFFLAP 1.0 model reproduced these results.

In summary, the interface test series provided a limited basis for testing our steady-state flow and fracture coupled model. It is likely that the rigid platen loading, and the elementray injection system contributed to the limitations of the test results.

Clearly, there was a need for a new, more sophisticated, series of tests to enable the validation of time-dependent analysis methods. Such tests were performed and are described next.

3. THE "LENS" TEST SERIES

3.1 Design and Fabrication of Test Blocks

The intention of this series of tests was to propagate a single-wing fracture of constant height through a sandstone lens embedded in a matrix of gypsum cement. To provide for straightforward numerical modeling, we attempted to keep the geometry of the tests simple. The fracture would extend in a plane perpendicular to the interface, and the interface would be perfectly bonded. The geometry of the sample was easy to control because the injection tube, sandstone tablet, and diagnostics such as tracking wires could be positioned in a mold before the gypsum was poured, and interface properties and angle could be changed easily. Gypsum cement is well characterized and had been used with the previous test series. Also, there is a significant contrast in material properties between the gypsum cement and the sandstone, not unlike that between the shales and the sandstones of the Western U.S. lenticular gas fields.

Blocks were constructed as shown in Figure 10. The hydrofracturing fluid was injected through a length of high pressure tubing that was slit on one side and wrapped with tape as shown in Figure 11. This configuration, in conjunction with the imposed stress field, caused a single-wing fracture to propagate from the injection tube to the sandstone tablet. To maintain constant height, the fracture was contained in the vertical direction by wire mesh screens embedded near the top and bottom of the block, and perpendicular to the injection tube.

Two sets of blocks were prepared, the mixture for both being 100 parts gypsum cement to 40 parts water. A first series of 4 blocks contained sandstone tablets, screen, and injection tubes. The sandstone tablets were seated on bolts, and tape was used to hold the tablets and the screens in position, while gypsum cement was poured. Dissection of these blocks showed their gypsum matrix to be heterogeneous and to contain large voids. We found that this was caused by the procedures used in mixing and pouring the gypsum cement. These blocks were used only for performance testing of the triaxial loading system, and will not be discussed further. The next series consisted of tests on 3 blocks which we will denote as Blocks A, B, and C. They contained the sandstone tablets, screen, injection tubes, and fracture-tracking wires. In these blocks, the screen and tablet were anchored using piano wire stretched

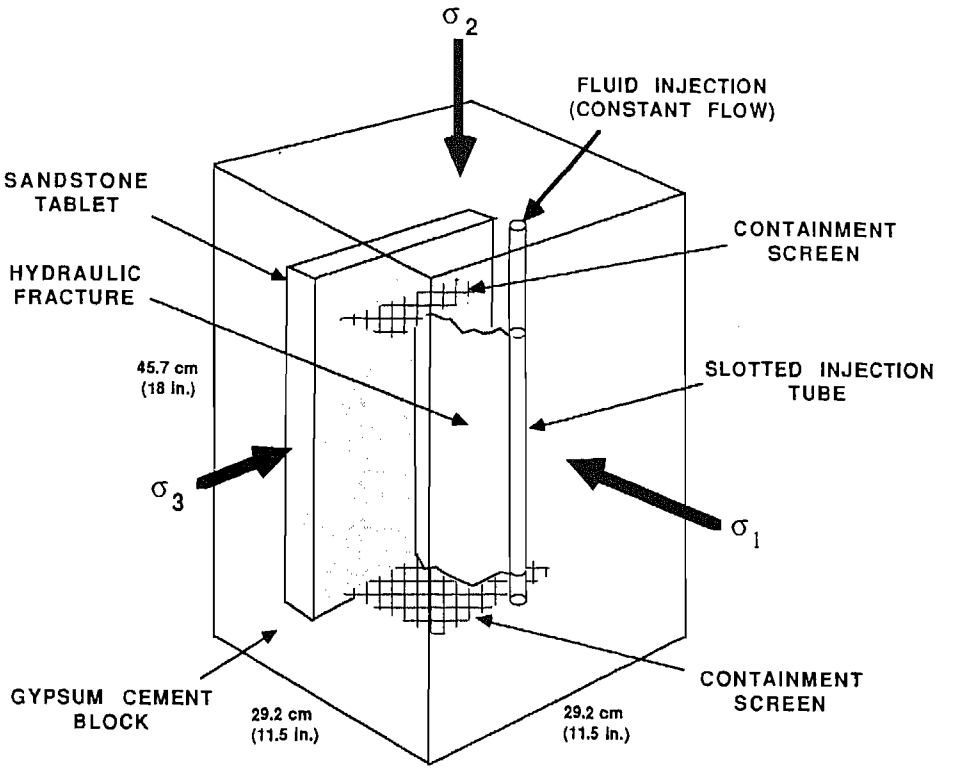

Figure 10. Schematic of Block-Fracturing Experiments.

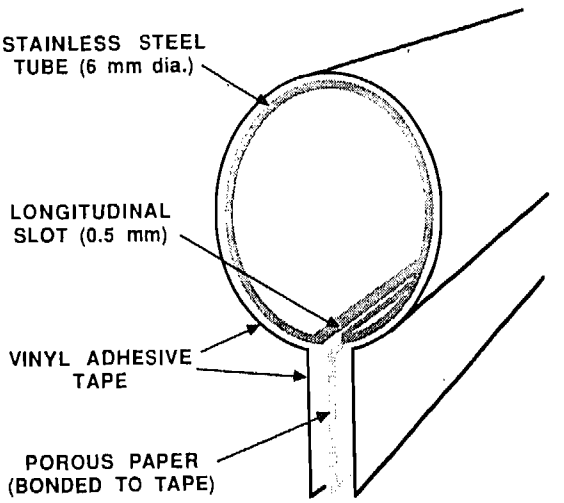

Figure 11. Cross-Section of Slotted Injection Tube.

across the mold, and the gypsum cement was prepared carefully, according to pre-planned procedures of sifting, wetting, mixing, and pouring. To improve texture, the blocks were also vibrated for 20 minutes after pouring. Dissection of the blocks after testing showed them to be very homogeneous.

3.2 Loading and Injection Systems

Blocks A, B, and C were tested in the apparatus shown schematically in Figure 12. The high-pressure cell consisted of a hardened steel cylinder that confines the block in the horizontal plane, and top and bottom platens that provide vertical confinement. Confining pressure was applied to each face of the block with flatjacks. The block and flatjacks were assembled in the confining cell, as shown in Figure 13. To aid in dissassembly, the flatjacks were coated with lubricant. Confining pressure was applied to the sample block by increasing the fluid pressure in the flatjacks using hydraulic hand pumps. Pressure on each set of opposing faces of the block was controlled independently to achieve a triaxial state of stress on the block. Each confining pressure system included a pressure gauge, pressure transducer, and pressure relief valve or burst disk.

Flatjacks used in the system were of two types. The first ones were a conventional design, with seams welded along the edges. Under cyclic loading and upon reuse, this type failed along the seams. To overcome this problem, we then used flatjacks fabricated following a new interior-seam design concept developed especially for this project (see Figure 14). These flatjacks performed very well under cyclic conditions. Their maximum expansion was of the order of 0.5 cm..

Injection fluid was supplied to the blocks at a constant rate using a high pressure pump that was also developed for this project. The pump (Figure 15) has positive displacement, with a total volume of one liter delivered at a maximum rate of 0.5 liter/min and a maximum pressure of 35 MPa. Injection rate is variable. The pump includes a pressure transducer, refill reservoir, pressure gauge, digital pressure readout, and control panel. The injection fluid used in the experiments was Mobil DTE light oil.

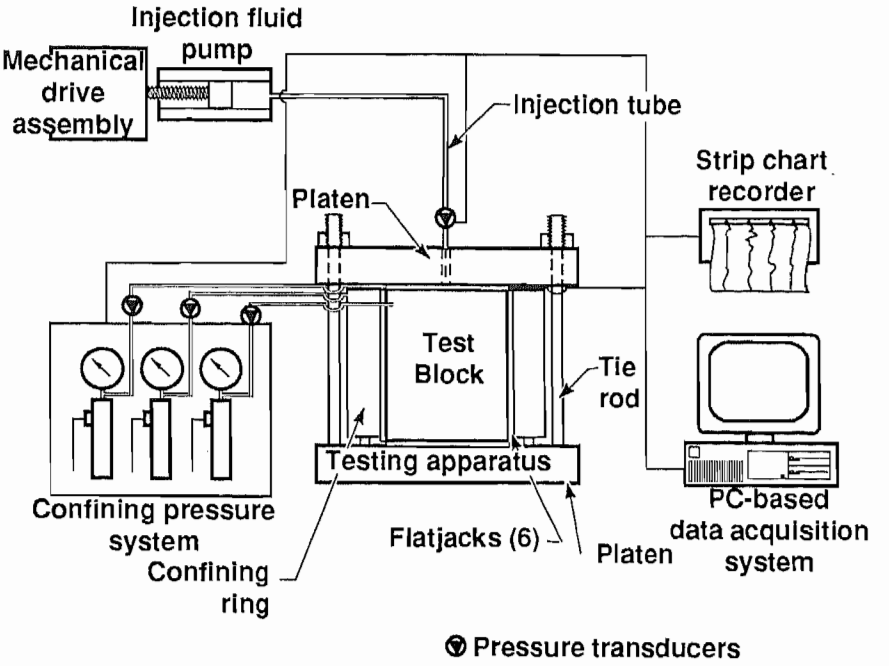

Figure 12. Schematic of Apparatus used to Conduct Block-Fracturing Experiments.

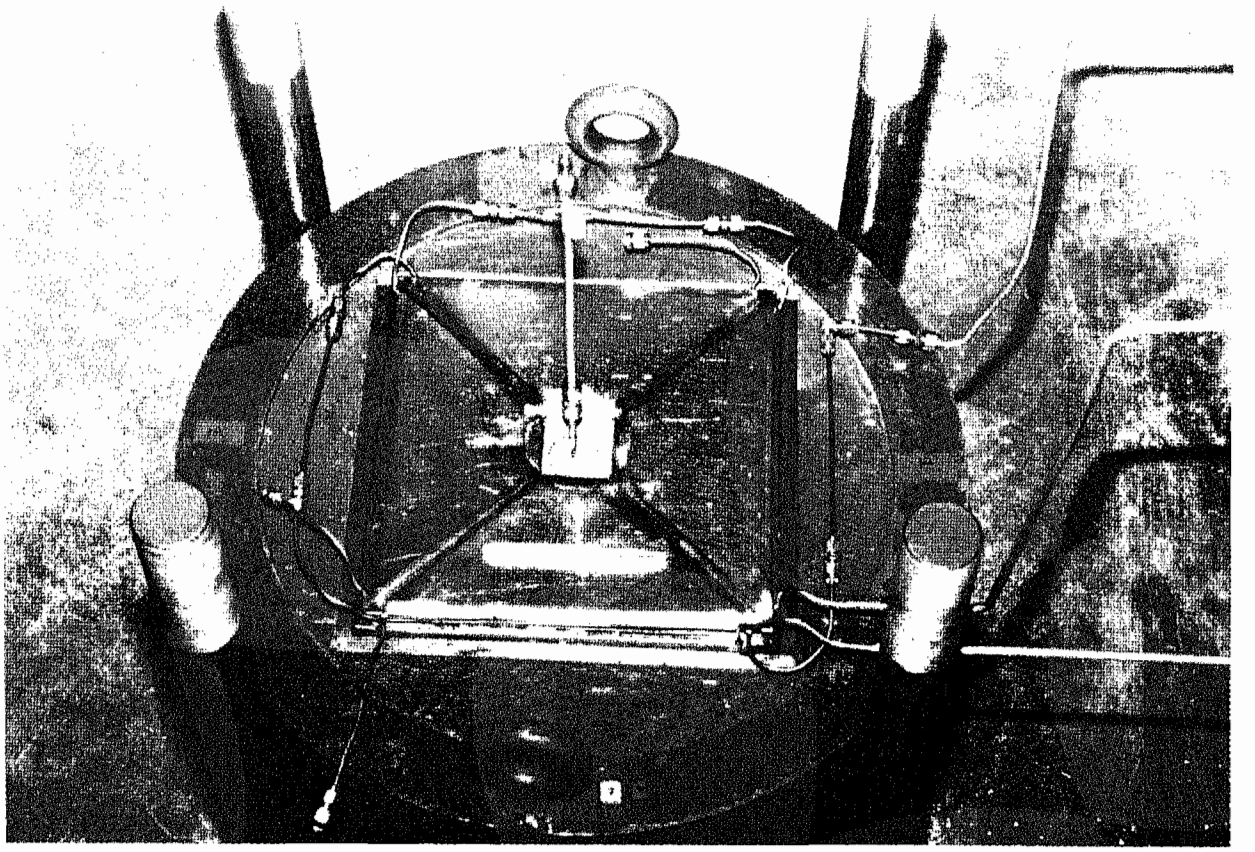

Figure 13. Top View of the Testing Frame with Gypsum Cement Block and Flatjacks in Place.

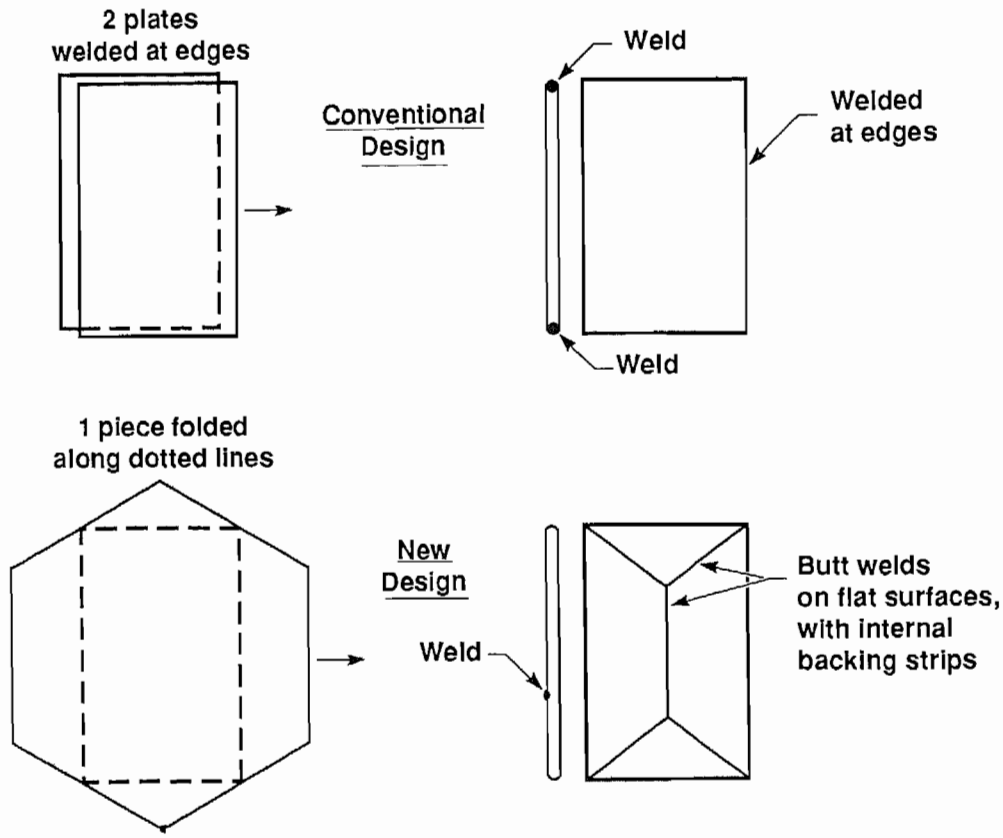

Figure 14. Design of Two Types of Flatjacks Used During the Experiments.

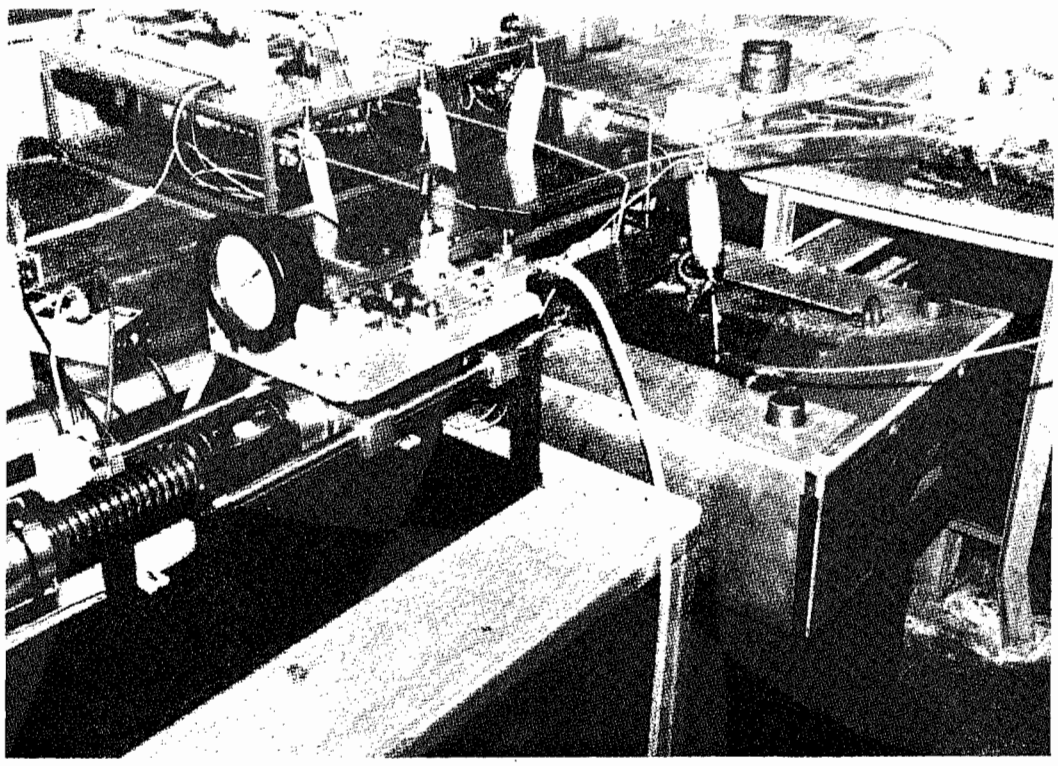

Figure 15. Fluid Injection System.

3.3 Fracture Tracking

To locate the crack front as a function of time, we designed a new technique for tracking fracture propagation in the gypsum blocks. This system uses very fine tungsten wires, .005 cm - .0076 cm diam, embedded in the blocks. Tungsten was chosen because of its brittle behavior. The wires are placed perpendicular to the proposed fracture plane and are designed to break when intersected by the fracture. The electrical continuity of the wires is monitored during the experiment and a sudden loss of continuity is taken to indicate intersection of a fracture with the wire. This method provides reliable information on the location of the crack front in space and time, is inexpensive to implement, and the data are easy to interpret. Because of its simplicity, we favored it over an earlier and more complex method involving embedded ultrasonic detectors [18].

To demonstrate the concept, we prepared two cylindrical samples 7.62 cm in diameter and 15.24 cm long, containing tracking wires, and then fractured them in Brazilian tensile tests. These samples were made of gypsum cement, and the wires were configured in the samples as shown in Figure 16. Results of these tests indicate that the wires broke at the initiation of fracture as estimated from the load-deformation records of the samples.

In addition, tracking wires were cast into two unlabeled blocks that were to be hydrofractured in unconfined conditions in order to test the tracking wires and the data acquisition system. However, while setting up the tests, we found that most of the tracking wires had lost electrical continuity. This was surprising, because we checked continuity periodically from the time the blocks were cast. We suspect that the wires were corroded by the dilute sulfuric acid solution given off during curing of the gypsum cement. We calculated the rate of corrosion of tungsten in such a solution, and found the lifetime of a .005 cm diam wire tube to be approximately 1 month, which coincided with the age of the blocks. Thus, we inferred this to be the cause of failure. In blocks A,B,C, wires were coated with a zinc-chromate primer to retard corrosion. We also monitored wire continuity closely during the curing period of the blocks, and scheduled testing of the blocks to be within a month of pouring. The arrangement of the wires in blocks A,B,C is shown in Figure 17. Four of the wires were positioned along the interface and two were placed between the injection tube and the interface.

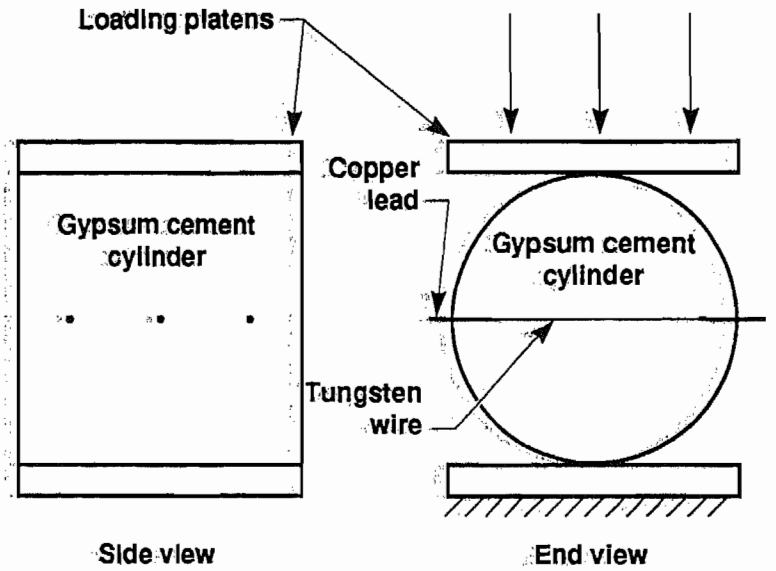

Figure 16. Schematic of Brazilian Tensile Test Showing Orientation of Tungsten Wires Used to Track Fracture.

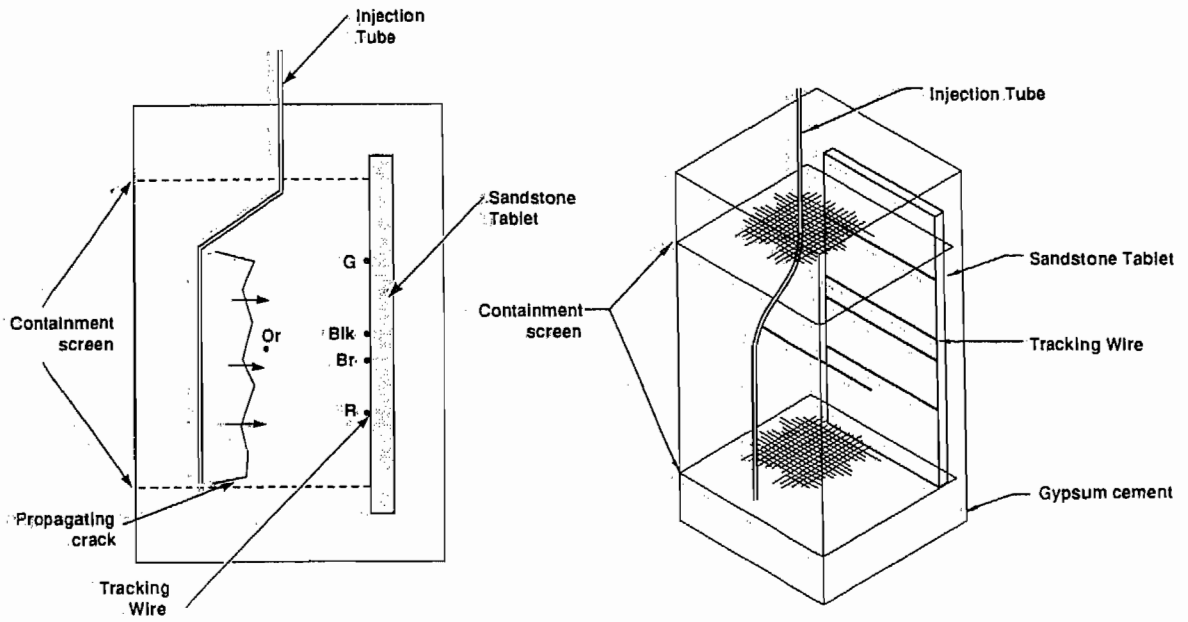

Figure 17. Orientation of Fracture-Tracking Wires in Gypsum Cement Blocks Containing Sandstone Tablets.

3.4 Data Acquisition and Reduction

A digital data acquisition system comprising an HP 3497 scanning digitizer coupled to an IBM-PCXT via a GPIB interface was developed and used for testing blocks A, B, and C. This system was configured to digitize and record 5 analog and 12 digital voltage signals with recording speeds of 400 μs/record. During tests A, B, and C, the recorded data included the three confining pressures, the injection pressure, and the continuity of six tracking wires. Confining and injection pressures were also recorded on strip chart or XY recorders. The system is shown in Figure 18.

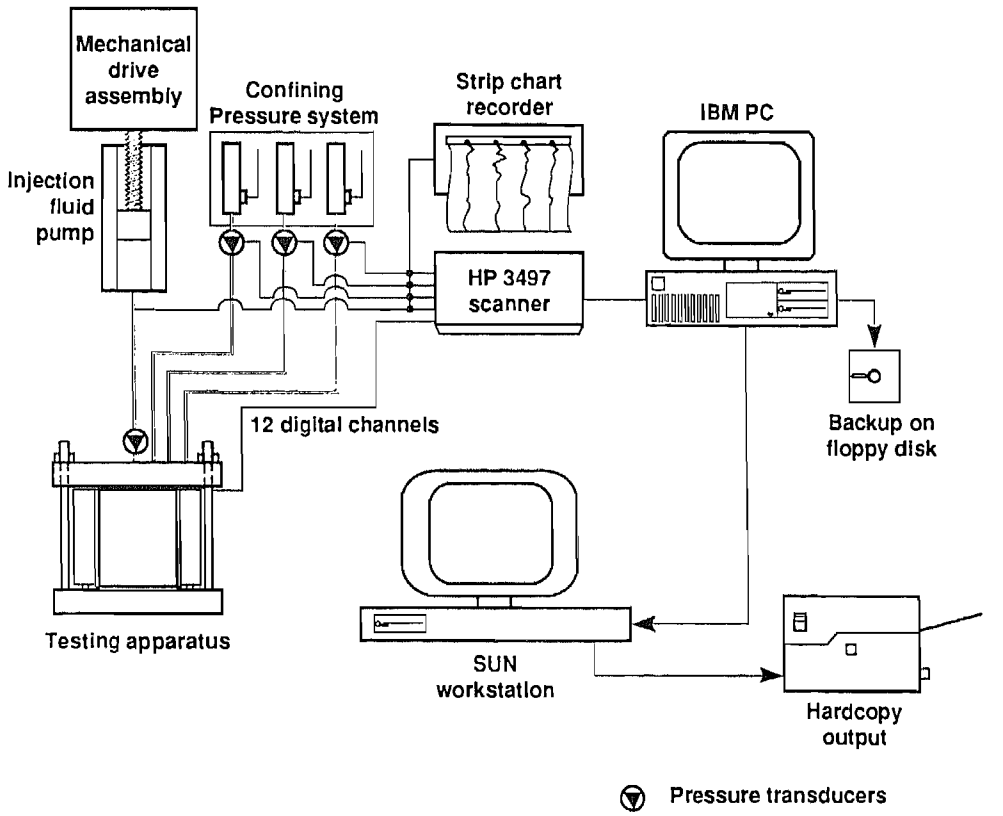

Figure 18. Schematic of System Used for Data Acquisition and Analysis.

The data were reduced using a SUN workstation and were backed up on a floppy disk. Voltage data were converted to pressure and analyzed using the LLNL SAC computer program [19].

3.5 Fracture Mapping

To determine the extent and nature of fracturing, each block was sectioned using a rock cutting saw. The blocks were cut into 5.1-cm thick slabs, in the horizontal plane. Fractures were highlighted using Partek, a fluorescent dye, and an ultraviolet light source. The geometry of the fracture and extent of fluid penetration were measured on each cross-section, recorded, and photographs were taken. These measurements of the fracture were then used to construct a fracture profile for each block.

3.6 Material Characterization

The mechanical properties of the sandstone and gypsum cement we used are summarized in Table 4.

Table 4. Mechanical and physical properties of test materials.

	Young's modulus (GPa)	Poisson's ratio, ν	Shear modulus GPa	Porosity ϕ (%)	Fracture toughness ($MPa \cdot m^{1/2}$)
Berea sandstone	20	0.38	7.2	18	1.1*
Gypsum cement	8.8	0.23	3.6	30	0.46

*value from reference [20].

3.7 Test Procedure

Initial conditions for tests A,B,C are listed in Table 5. The confining stresses and fluid injection rate were held constant during the tests. The procedure for each test was to (1) raise confining stress on all faces of the block simultaneously to the least principal stress, (2) raise the maximum and intermediate stresses to the intermediate stress level, and (3) raise the maximum stress to the desired level. After the confining stresses were applied, injection fluid was introduced into the injection tube and injection pressure was

raised to 0.69 MPa and held constant for a few minutes. Injection pressure was then reduced to zero. This procedure served to saturate the gypsum in the region immediately surrounding the injection tube. The test was then initiated by starting the data acquisition system and the fluid injection pump.

Table 5. Test conditions for blocks A, B, and C.

Maximum principal stress	σ_1	10.34 MPa
Intermediate principal stress	σ_2	6.90 MPa
Minimum principal stress	σ_3	2.07 MPa
Injection rate	Q	0.16 l/min.

3.8 Test Results

Some key features of the three tests are summarized in Table 6, and a more detailed discussion of pressure records and fracture behavior follows.

Table 6. Key elements of block test results.

Block	Crack height (cm)	Crack length (cm)	Crack area (cm^2)	Peak pressure (MPa)	Duration of injection (s)	Duration of irregular leakoff (s)	Fluid penetration into sidewall (cm)
A	25.4	19.7	513	18.6	360	60	2.5
B	22.9	19.1	432	16.4	343	-	3.2
C	26.7	24	571	17	382	65	2.5

3.8.1 Pressure-time records

Block A

The record of injection pressure-time for Block A is shown in Figure 19a. It has a well-defined peak or breakdown pressure of approximately 18.6 MPa. After breakdown, the injection pressure drops sharply for about 15 s, then decays in a smooth and gradual manner for about 60 s. At t = 75 s, pressure response becomes irregular and the rate of

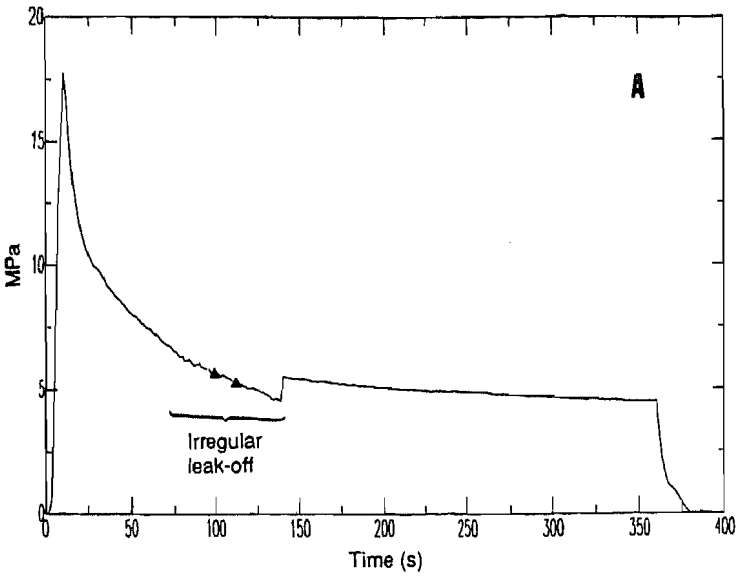

a) Block A

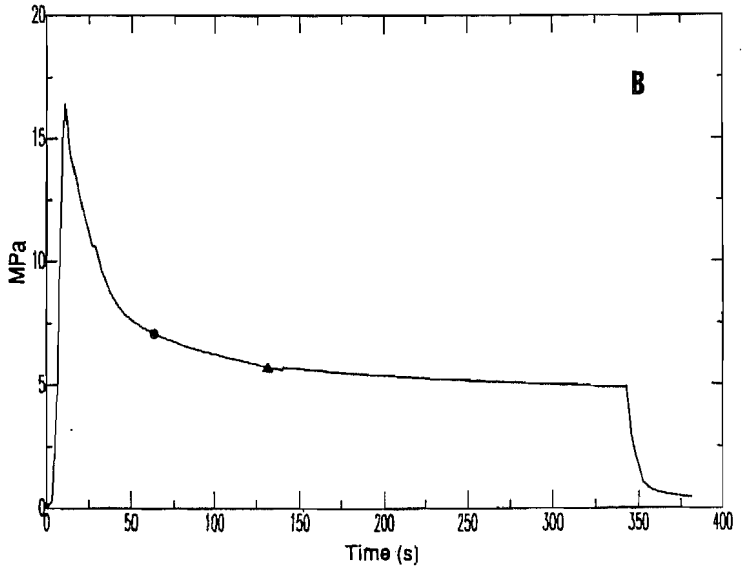

b) Block B

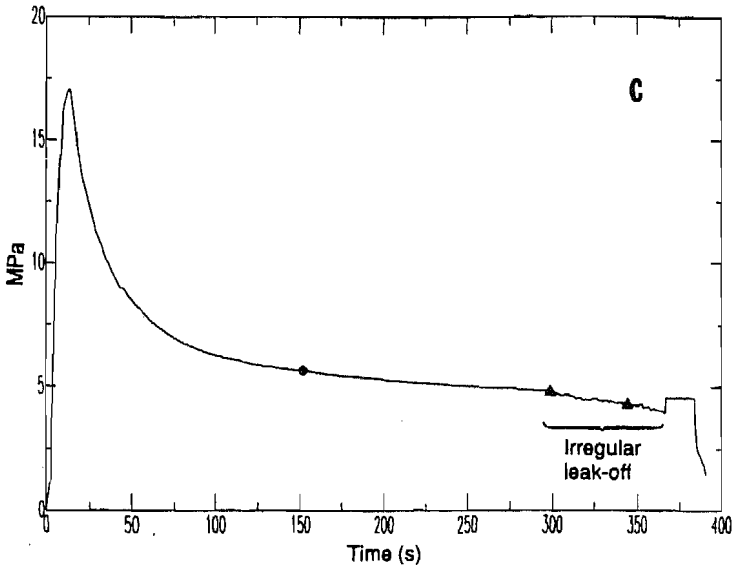

c) Block C

Figure 19. Records for Block Tests A, B, and C.

decay decreases until t = 135 s, when there is a sudden increase in pressure. After this, pressure decreases steadily until the end of injection at t = 360 sec.

Times at which the tracking wires at the interface lost continuity are tabulated in Table 7, and are plotted as solid triangles in Fig. 19a. Notice that the wires broke during the period of irregular leak-off before the step increase, and that the (brown) wire nearest the horizontal midplane of the block broke first.

Table 7. Fracture tracking data, showing elapsed time (seconds) from start of injection to loss of continuity for fracture tracking wires. Wire locations are shown in Figure 17.

	Elapsed Time (s)				
	Orange	Brown	Red	Green	Black
A	-	100	-	113	-
B	63	130	-	-	-
C	151	-	343	-	296

Block B

The injection pressure-time record for Block B is shown in Figure 19b. These data are similar to those for test A. Again, a step increase occurs at about t = 135 s. After the step increase, pressure decreases slowly and steadily with increasing time. As in block A, the wire located near the interface (solid triangle) broke prior to the step increase in pressure at 135 s. The solid circle shows breakage of the wire embedded between the injection tube and the tablet. A crack propagation velocity of 0.07 cm/s was estimated from the tracking data.

Block C

Figure 19c shows features similar to those of the previous two tests. Notice that, as in test A, wires located at the interface (solid triangles) broke during the period of irregular leak-off just prior to the step increase, and the (black) wire located nearest the horizontal midplane of the block broke first. A fracture propagation velocity of 0.041 cm/s was estimated from the tracking wires. This is somewhat slower than the velocity estimated for block B, and may be due to small differences in permeability between the blocks. The calculations in the companion paper clearly show the sensitivity of fracture propagation speed to block permeability.

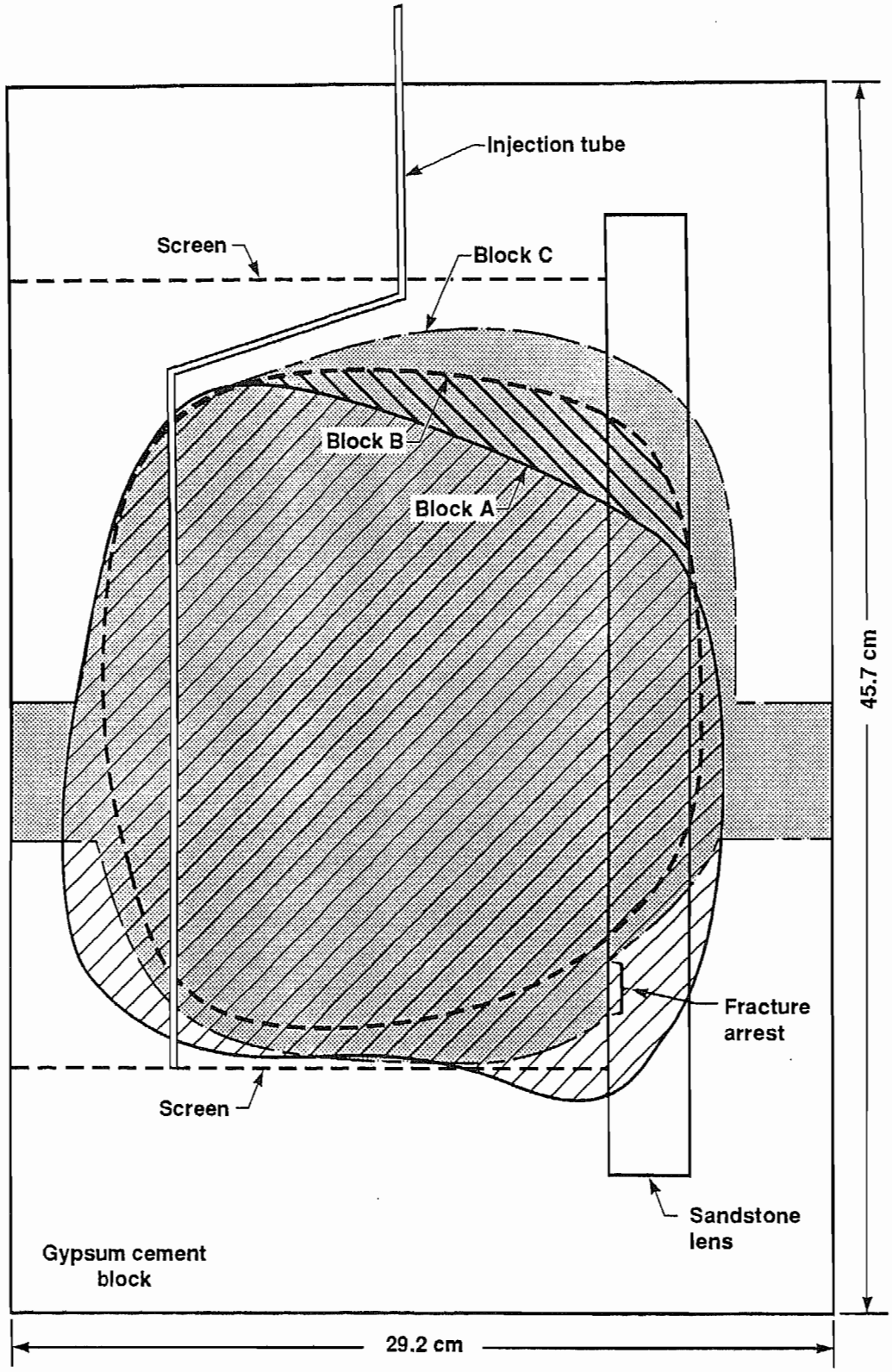

Figure 20. Map of Fracture Planes for Blocks A, B, and C. Note that all Fractures Penetrated the Sandstone and Were Confined in the Vertical Direction. Fracture in Block C was Arrested Along the Lower Portion of the Interface.

3.8.2 Mapping of fractures

As introduced earlier, the blocks were cut into 5-cm thick slabs in the horizontal plane and the fractures were mapped from these slabs using fluorescent Partek dye and ultraviolet light. Fracture cross-sections for the three blocks are drawn in Figure 20. This figure shows that the fractures produced in these blocks are similar in size. The figure also shows that each fracture penetrated the sandstone lens, and that the vertical extent of the hydrofracture propagation was limited by the mesh screens embedded in the gypsum cement. Vertical confinement is important for code validation, since FEFFLAP assumes a fracture of constant height. Figure 20 also shows that the fracture produced in block B had the smallest penetration of the sandstone. This is interesting because, as noted in the pressure record, the increase in the injection pressure associated with the interface was much smaller than that observed for blocks A and C. Figure 20 shows that the fracture in block C was arrested along the lower portion of the gypsum/sandstone interface. Further evidence of crack arrest at the interface for block C is shown in Figure 21, where we see that the fracture exhibited lateral steps as it entered and exited the sandstone tablet. The curved shape of the crack front in each test, shows that the fracture propagated furthest in the horizontal midplane of the sample. This is consistent with the tracking data which indicate that the fracture first reached the interface at the horizontal midplane of the block.

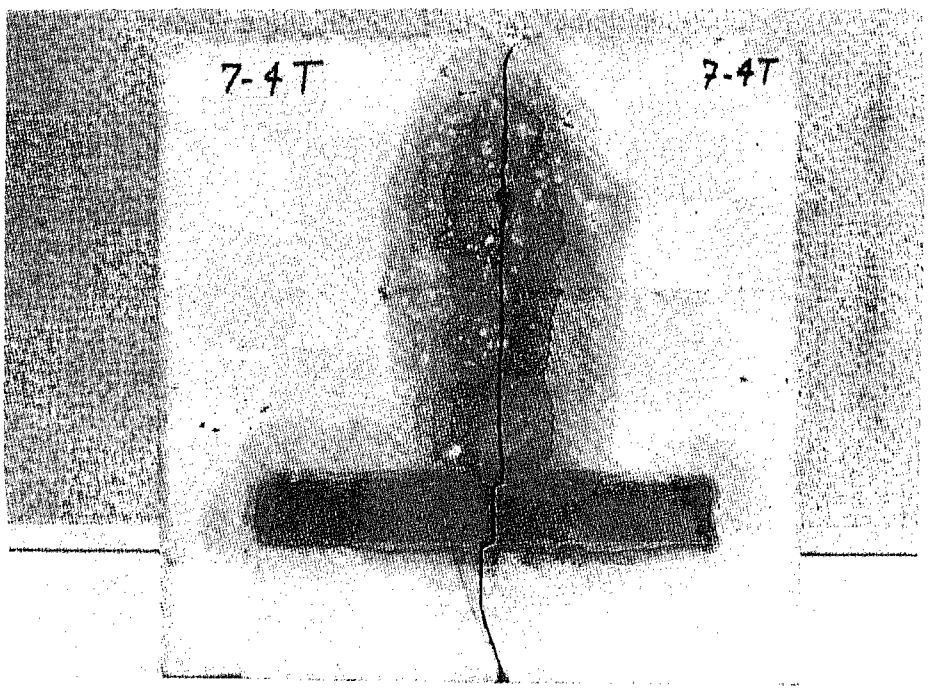

Figure 21. Cross Section Through Center of Block C. Note Steps in the Fracture as it Entered and Exited the Sandstone Tablet.

3.9 Discussion

From the pressure-time records and tracking wire data we determined that wires located near the discontinuity broke during periods of irregular leak-off (blocks A and C) and that opening of the fracture at the interface was initiated in the horizontal midplane of the block. For all three tests, a step increase in pressure occurred after wires located at the interface lost continuity. It is important to note that the data from the tracking wires show that for blocks A and C, the fracture was extending vertically along the interface during the period of irregular leak-off. For block B we know that the fracture was open at the interface before the step increase, based on the breakage of a tungsten wire.

We propose the following scenario to explain these results (Figure 22). After breakdown, the fracture propagates smoothly in the gypsum cement, but it stops upon reaching the sandstone lens. This is because increased energy is required to drive the fracture in the sandstone as it has higher values of fracture toughness and critical energy release rate than the gypsum. As injection continues, the crack spreads along the interface between the gypsum and the sandstone, and causes stick slip sliding and some fluid flow along the interface. This would result in an irregular pressure response caused by crack extension along the interface and stick slip behavior, and an increased rate of leakoff as fluid gains access to the more permeable sandstone. As the sandstone becomes nearly saturated with oil, leakoff is again controlled by the permeability of the gypsum cement, and pressure rises sharply until stress is sufficient to continue growth of the hydrofracture into and through the sandstone tablet.

4. SUMMARY

Our experimental program has fulfilled its purpose. In particular, the triaxially loaded test series yielded important results on two fronts: it enabled a measure of validation of the coupled fracture and flow numerical model for transient fracture behavior, and it provided a physical basis for the conclusion that pressure-time records would reflect the interaction of induced fractures with natural fractures. This is a significant step in the search for better diagnostics of underground hydrofracture behavior. Also, we have introduced new techniques for initiating, containing, and tracking hydraulic fractures; and we have contributed an improved design for hydraulic flatjacks.

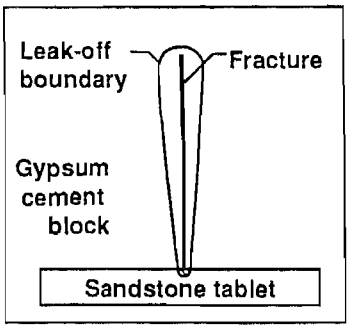

Fracture from the borehole has reached the sandstone tablet. Fluid is diffusing into the gypsum block. The width of the fracture is exaggerated in all frames, for clarity.

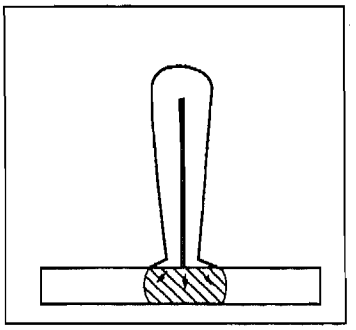

At the interface, fluid percolates into sandstone, and starts flowing along the interface. No cracking in tablet yet.

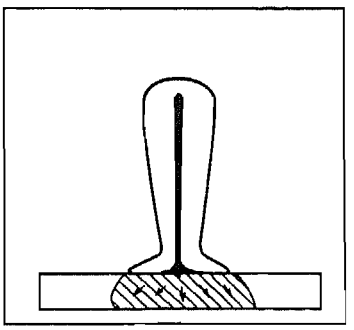

Under some conditions of confining stress and borehole pressure, a fracture is initiated into the sandstone.

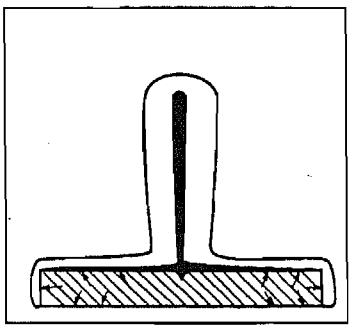

Meanwhile, fluid continues to leak-off into the gypsum cement, along the interface, and into the sandstone.

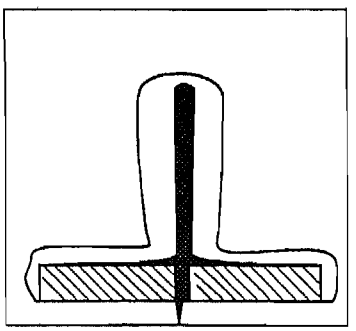

When the more permeable sandstone tablet becomes saturated, the cracking continues through the sandstone. The fracture may show offsets upon entry and/or exit of the tablet (see Figure 21).

Figure 22. Hypothesized Sequence of Fracture Propagation and Fluid Flow During the Block Tests with Embedded Sandstone Tablets, Viewed from Above.

Certainly this type of physical testing could be expanded. Additional laboratory tests that would extend the data base and allow more detailed analysis are warranted. In particular, one would determine the pressure-time response for fractures that inflate a material interface but do not cross it. One would also study the effect of fluid properties on fracture behavior at interfaces by conducting tests using injection fluids with different compressibilities and/or viscosities. One would vary the angle of intersection of the hydrofracture and the sandstone lens, and the bonding of the lens to the hydrostone. These additional physical tests would form a comprehensive data base to fully validate the numerical models, which in turn can be used to simulate many other possible situations of interest in fluid-driven fracturing.

5. REFERENCES

1. Lamont, N. and Jessen, F. (1963) "The Effects of Existing Fractures in Rocks on the Extension of Hydraulic Fractures", J. Pet. Tech., Feb., pp. 203-209.

2. Daneshy, A. A. (1974) "Hydraulic Fracture Propagation in the Presence of Planes of Weakness", SPE Preprint 4852, SPE-European Spring Mtg., Amsterdam, May.

3. Hanson, M. E., Anderson, G. D., and Shaffer, R. J. (1980) "Theoretical and Experimental Research on Hydraulic Fracturing", ASME J. of Energy Resources Recovery, v. 102, pp. 92-98, June.

4. Hanson, M. E., Anderson, G. D., Shaffer, R. J., and Thorson, L. D. (1981) "Some Effects of Stress, Friction, and Fluid Flow on Hydraulic Fracturing", SPE Preprint 9831, SPE/DOE Symposium on Unconventional Gas Recovery, Denver, CO, March. Also Lawrence Livermore National Laboratory Report UCRL-85003.

5. Blanton, T. L. (1982) "An Experimental Study of Interaction Between Hydraulically Induced and Pre-Existing Fractures", SPE Preprint 10847, SPE/DOE Symposium on Unconventional Gas Recovery, Denver, CO, March.

6. Ahmed, U., Strawn, J., Wilson, M. and Schatz, J. (1983) "Effect of Stress Distribution on Hydraulic Fracture Geometry: A Laboratory Simulation Study in One Meter Cubic blocks", SPE Preprint 11637, SPE/DOE Symposium on Low Permeability, Denver, CO, March.

7. Thorpe, R. K., Heuze, F. E., and Shaffer, R. J. (1984) "An Experimental Study of Hydraulic Fracture - Interface Interaction", Lawrence Livermore National Laboratory, UCID-20114, 27 p., July.

8. Swift, R. P., and Kusubov, A. S. (1982) "Multiple Fracturing of Boreholes by Using Tailored-Pulse Loading", J. Soc. Petroleum Eng., pp 923-932, Dec.

9. Blanton, T., Thompson, T. W., and Mann, K. L. (1986) "Analysis of Fracturing Mechanisms in Naturally Fractured Rocks", Final Report to U.S. Department of Energy, Morgantown, WV, by Science Applications Int. Corp., San Diego, CA, Contract DE-AC21-83MC20289.

10. Schatz, J., Zeigler, B. J., Bellman, R. A., Hanson, H. M., Christianson, M., and Hart, R. D. (1987) "Prediction and Interpretation of Multiple Radial Fracture Stimulations", Final Report by Science Applications Int. Corp., San Diego, CA, to Gas Research Institute, Chicago, IL, Report GRI-87-0199.

11. Blair, S. C., Thorpe, R. K., and Heuze, F. E. (1988) "Physical Models of Hydrofracturing Across Material Interfaces", Lawrence Livermore National Laboratory, UCID-21505, 28 p., October.

12. Shaffer, R. J., Thorpe, R. K., Ingraffea, A. R., and Heuze, F. E. (1984) "Numerical and Physical Studies of Fluid-Driven Fracture Propagation in Jointed Rock", Proc. 25th U.S. Symp. rock Mechanics, Evanston, IL, pp 117-126, (Soc. Mining Eng., Littleton, CO).

13. Ingraffea, A. R., Gunsallus, K. L., Beech, J. F., and Nelson, P. P. (1984) "A Short-Rod Based System for Fracture toughness Testing of Rock", STP No. 855, ASTM Symposium on Chevron-Notched Specimens: Testing and Stress Analysis.

14. Ingraffea, A. R., Perucchio, R., Han, T.-Y., Gerstle, W. H., and Huang, Y. P. (1984) "Three-Dimensional Finite and Boundary Element Calibration of the Short-Rod Specimen", STP No. 855, ASTM Symposium on Chevron-Notched Specimens: Testing and Stress Analysis.

15. Ingraffea, A. R., Shaffer, R. J., and Heuze, F. E. (1985) "FEFFLAP: A Finite Element Program for Analysis of Fluid-Driven Fracture Propagation in Jointed Rock. Vol. 1: Theory and Programmer's Manual", Lawrence Livermore National Laboratory, UCID-20368, March.

16. Shaffer, R. J., Ingraffea, A. R., and Heuze, F. E. (1985) "FEFFLAP: A Finite Element Program for Analysis of Fluid-Driven Fracture Propagation in Jointed Rock. Vol. 2: User's and Verification Manual", Lawrence Livermore National Laboratory, UCID-20369, March.

17. St. John, C. M. (1971) "Three-Dimensional Analysis of Rock Slopes", Proc. Symp. Int. Soc. Rock Mech., Nancy, France, Sept.

18. Heuze, F., Shaffer, R., Thorpe, R., and Wijesinghe, A. (1987) "Fracture Mechanics Research at LLNL", Proceedings Unconventional Gas Recovery Contractors Review Meeting, Morgantown, WV, DE 87-006490, pp. 270-279, July.

19. Tull, J. E., (1986) "SAC, A Signal Processing System for Research Seismology", Lawrence Livermore National Laboratory, UCRL-94153, May.

20. Thiercelin, M. (1987) "Fracture Toughness under Confining Pressure Using the Modified Ring Test", Proc. 28th U.S. Symposium on Rock Mech., Tucson, pp. 149-156, (A. A. Balkema, Brookfield, VT).

6. ACKNOWLEDGMENTS

This work was performed by the Lawrence Livermore National Laboratory under Contract W-7405-Eng-48 with the U. S. Department of Energy, as coordinated through the Morgantown Energy Technology Center.

We thank L. Grabowski for her fine typing of the manuscript, Professors R. Goodman and N. Cook (U.C. Berkeley) for their technical advice, and C. Witherell (LLNL) for the new flatjack concept.